

Indirect combustion noise

M. S. HOWE†

College of Engineering, Boston University, Boston, MA 02215, USA

(Received 18 November 2009; revised 8 April 2010; accepted 21 April 2010;
first published online 20 July 2010)

An analysis is made of the noise generated during the passage of quiescent temperature/entropy inhomogeneities through regions of rapidly accelerated mean flow. This is an important source of jet engine core noise. Bake *et al.* (*J. Sound Vib.*, vol. 326, 2009, pp. 574–598) have used an ‘entropy wave generator’ coupled with a converging–diverging nozzle to perform a series of canonical measurements of the sound produced when the inhomogeneity consists of a nominally uniform slug of hot gas. When flow separation and jet formation occur in the diffuser section of the nozzle, it is shown in this paper that the vortex sound generated by the jet is strongly correlated with the entropy noise produced by the slug and that the overall noise level is significantly reduced. Streamwise ‘stretching’ of the hot slug during high subsonic acceleration into the nozzle and the consequent attenuation of the entropy gradient in the nozzle are shown to significantly decrease the effective rate at which indirect combustion noise increases with the Mach number. Numerical predictions indicate that this is responsible for the peak observed by Bake *et al.* in the entropy-generated sound pressure at a nozzle Mach number near 0.6.

Key words: aeroacoustics, gas dynamics, instability

1. Introduction

Unsteady combustion is a major source of the noise produced by gas turbines, industrial furnaces and other propulsive devices (Strahle 1971, 1978; Crighton *et al.* 1992; Poinsot & Veynante 2005; Leyko, Nicoud & Poinsot 2009). Freely burning gas constitutes an acoustic ‘monopole’ source of strength determined by the volumetric rate of expansion in the combustion zone, a mechanism whose efficiency is greatly increased by the stretching of flame fronts by turbulence velocity fluctuations (Strahle 1978). This noise is frequently augmented in confined systems by secondary or ‘indirect’ combustion sources that arise during acceleration of unevenly heated combustion products through the system exhaust and is manifested as a ‘dipole’ acoustic source involving interactions between temperature ‘hot spots’ and mean flow variations. The dipole strength is proportional to the force perturbation needed to accelerate temperature disturbances at the same rate as the surrounding gas. It is often called ‘entropy noise’ and was first investigated analytically at low Mach numbers by Candel (1972), Marble (1973) and Morfey (1973) and later by Ffowcs Williams & Howe (1975), Howe (1975) and Lu (1977); numerical treatments at higher Mach numbers were given by Bohn (1977), Cumpsty & Marble (1977*a, b*), Marble & Candel (1977), Cumpsty (1979) and Bloys (1979). The application of Marble & Candel (1977) to high-Mach-number nozzle flow was based on a linearization of the

† Email address for correspondence: mshowe@bu.edu

unsteady motion that treated the nozzle as a compact element across which flow quantities varied discontinuously. The method was extended by Cumpsty & Marble (1977*a, b*) and Cumpsy (1979) to study entropy noise produced in a gas turbine at the combustor outlet and turbine blade stages. The outlet flow is usually ‘choked’, and the indirect combustion noise is therefore related to the unsteady volume or mass flux occurring when temperature inhomogeneities enter the outlet throat, producing fluctuations in the choked sound speed. Muthukrishnan, Strahle & Neale (1978) deduced from experiments with choked nozzles that indirect entropy noise is the principal source of the engine ‘core noise’. It was concluded for such flows by Leyko *et al.* (2009) that the linearized acoustic theory of Marble & Candel (1977) agrees well at very low frequencies with numerical predictions made using the Euler equations of motion, provided all length scales (including that of the entropy disturbances) are much larger than the nozzle.

According to Bake, Michel & Rohle (2007), a proper analytical understanding of the indirect noise source is still lacking and can be obtained only by a comparison of theoretical predictions with careful experiment. To do this they and Bake *et al.* (2009*a, b*) performed a series of canonical experiments using an ‘entropy wave generator’. These involved the measurement of the sound generated during controlled high-speed convection of a slug of hot gas through a converging–diverging nozzle. The hot slug is regarded as an idealized product of combustion, and it is argued that a study of the sound-source mechanism in this case should provide improved insight into the production of sound by a real inhomogeneous combustion outflow. The experiment is a much-improved and sophisticated version of a similar arrangement used previously by Zukoski & Auerbach (1976) and Bohn (1977) at the California Institute of Technology, in which, however, the temperature excess of the slug was limited to about 1 K.

Bake *et al.* (2009*b*) asserted that indirect combustion noise is dipole in character and that its mechanism of generation must be similar to that produced by turbulence and other vortex sources in confined flows, so that the overall contributions from the two sources are not independent and should not be considered in isolation. However, their numerical simulations were incapable of quantifying the separate effects of the entropy and vortex sources in their experiment. Such coupling of thermal and vortex sources is included in the widely used linear theory of Marble & Candel (1977), but according to Bake *et al.* (2009*a*), predictions are too low at nozzle Mach numbers M_t less than about 0.6 and too high when $M_t > 0.7$. Numerical and analytical methods for the supersonic case have been discussed by Leyko *et al.* (2009) and by Muhlbauer, Noll & Aigner (2009).

The experiments of Bake *et al.* (2009*b*) are the motivation for the reappraisal of the earlier theoretical work on indirect combustion noise discussed in this paper. The general entropy noise problem is formulated in the context of these experiments in §§2 and 3. Application is made in §4 to determine the indirect combustion noise generated when an ideal slug of hot gas (i.e. one having sharp-fronted interfaces with the ambient flow) convects at high subsonic speed through a converging–diverging nozzle. The results are extended to include the possible impact on the generated sound of large-scale separation of the flow from the wall of the nozzle diffuser, leading to the conclusion that the additional contribution from vortex sound sources causes an overall reduction in the entropy noise. In both cases the indirect combustion noise is predicted to increase with the throat Mach number M_t for an idealized hot slug, in qualitative agreement with data reported by Bake *et al.* (2009*b*) for $M_t < 0.6$. According to experiment, however, the peak acoustic pressure stops

increasing at $M_t \sim 0.6$, beyond which there is a levelling off and a small decrease, and flow separation apparently does not occur. Vorticity production in the nozzle cannot, therefore, account for this decrease. The discrepancy between theory and experiment is discussed in detail §5, where it is argued that peak pressure saturation occurs because of the progressive increase with the Mach number of the thickness of the slug ‘interface’, across which the temperature rises from the local ambient temperature to that of the hot slug. This increase is produced by stretching of the transition region during convection through the rapidly accelerated nozzle mean flow, an effect that is exacerbated by the increasing flow Mach number. Excellent agreement with the data of Bake *et al.* (2009*b*) is obtained when the finite thickness of the slug transition zone is taken into account, although there remains some uncertainty about the extent to which wavefront thickness was properly controlled in the experiments.

2. The governing equations

2.1. Equation of aerodynamic sound

Sound in a fluid with stationary boundaries is generated by unsteady distributions of vorticity and by their interactions with the boundaries and by thermodynamically irreversible phenomena usually associated with combustion. The hot and thermodynamically inhomogeneous flow in a jet engine or rocket motor occurs at a sufficiently large Reynolds number such that the transfer of momentum and heat by molecular diffusion within the body of the flow can usually be neglected. This generally implies that the dominant fluid motions occur isentropically and that all effects of molecular diffusion are confined to low-velocity regions immediately adjacent to solid boundaries.

Consider a perfect gas and take the momentum equation governing the motion at $\mathbf{x} = (x, y, z)$ within the fluid at time t in Crocco’s form (Howe 1998):

$$\frac{\partial \mathbf{v}}{\partial t} + \nabla B = -\boldsymbol{\omega} \wedge \mathbf{v} + T \nabla s - \frac{\eta}{\rho} \text{curl } \boldsymbol{\omega}, \quad (2.1)$$

where \mathbf{v} is the velocity; $\boldsymbol{\omega} = \text{curl } \mathbf{v}$ is the vorticity; ρ , T and s are respectively the density, temperature and specific entropy; and η is the shear coefficient of viscosity. Further, B is the total enthalpy:

$$B = c_p T + \frac{1}{2} v^2, \quad (2.2)$$

where c_p is the ratio of specific heats at constant pressure. It is assumed in (2.1) that viscous effects are important only near boundaries, and only the principal viscous shear stress term has been retained.

Multiply (2.1) by the density ρ and take the divergence, to obtain

$$\text{div} \left(\rho \frac{\partial \mathbf{v}}{\partial t} \right) + \text{div}(\rho \nabla B) = -\text{div}(\rho \boldsymbol{\omega} \wedge \mathbf{v} - \rho T \nabla s), \quad (2.3)$$

provided η may be taken to be constant. This is transformed into an acoustic analogy equation (Lighthill 1952; Howe 1998) for B by the procedure described in detail by Howe (2002, §5.2.1) for the simpler case of homentropic flow (where $s = \text{constant}$).

The equation of continuity and the thermodynamic relation $c_p dT = dp/\rho + T ds$, where p denotes pressure, are used to show (without approximation) that

$$\text{div} \left(\rho \frac{\partial \mathbf{v}}{\partial t} \right) = -\rho \frac{D}{Dt} \left(\frac{1}{\rho} \frac{\partial \rho}{\partial t} \right) \equiv -\rho \frac{D}{Dt} \left(\frac{1}{\rho c^2} \frac{\partial p}{\partial t} \right) + \rho \frac{D}{Dt} \left(\frac{\beta T}{c_p} \frac{\partial s}{\partial t} \right), \quad (2.4)$$

where c is the speed of sound; $\beta = (-1/\rho)(\partial\rho/\partial T)_p$ is the coefficient of expansion; and $D/Dt = \partial/\partial t + \mathbf{v} \cdot \nabla$ is the material derivative. Similarly, the momentum equation (2.1) supplies the relation

$$\frac{1}{\rho} \frac{\partial p}{\partial t} = \frac{DB}{Dt} - T \frac{Ds}{Dt} + \frac{\eta}{\rho} \mathbf{v} \cdot \text{curl } \boldsymbol{\omega}. \quad (2.5)$$

For isentropic flow $Ds/Dt = 0$ and viscous effects can be neglected in the body of the fluid, so that when (2.4) and (2.5) are used to replace the first term on the left-hand side of (2.3) we find that

$$\left(\rho \frac{D}{Dt} \left(\frac{1}{c^2} \frac{D}{Dt} \right) - \frac{\partial}{\partial x_j} \left(\rho \frac{\partial}{\partial x_j} \right) \right) B = \text{div}(\rho \boldsymbol{\omega} \wedge \mathbf{v} - \rho T \nabla s) + \rho \frac{D}{Dt} \left(\frac{\beta T}{c_p} \frac{\partial s}{\partial t} \right), \quad (2.6)$$

where the repeated subscript j implies summation over all three spatial coordinates.

In the absence of vorticity and entropy fluctuations, and of moving boundaries, Bernoulli's equation implies that the total enthalpy B is constant throughout the flow. In the more general, unsteady case the motion outside the region occupied by vorticity and entropy inhomogeneities is irrotational, and the corresponding variations in B are equal to $-\partial\varphi/\partial t$, where $\varphi(\mathbf{x}, t)$ is a suitable velocity potential. The right-hand side of (2.6) therefore identifies the vortex and entropic sources responsible for these variations, which vanish in their absence. The final term on the right-hand side represents a predominantly monopole source arising from volumetric expansion of the fluid in the source region produced, for example, by heat addition. The divergence term accounts for the production of sound by the vortex motions and entropy gradients, the latter serving to 'scatter' near-field pressure fluctuations ($p = \rho RT$, where R is the gas constant) into sound. In the acoustic region (2.5) indicates that fluctuations in B are related to the acoustic pressure by

$$\frac{1}{\rho} \frac{\partial p}{\partial t} = \frac{DB}{Dt}. \quad (2.7)$$

This reduces to $p \simeq \rho_o B \equiv -\rho_o \partial\varphi/\partial t$ when the far-field, mean flow Mach number is very small, where ρ_o is the corresponding mean density.

The coefficients in the differential operator on the left-hand side of (2.6) account for nonlinear effects of propagation because local values of ρ , c and the flow velocity \mathbf{v} are strictly dependent on the acoustic disturbance. In a general, large-scale turbulent flow spanned by many characteristic acoustic wavelengths, the vortex source and entropy sources are also responsible for the scattering and refraction of sound. However, in order to calculate the radiation to first order in the entropy perturbation it is sufficient to replace ρ , c and \mathbf{v} where they appear on the left-hand side of (2.6) by their local mean values. Similarly, the final monopole source on the right-hand side vanishes to first order in the perturbation entropy.

2.2. Application to indirect combustion noise generated by an ideal slug of hot gas

Equation (2.6) will be used to examine the generation of sound during the passage of a hot slug of gas through a nozzle in a high-speed duct flow. The mathematical problem is illustrated schematically in figure 1 and is intended to model the production of indirect combustion noise in the entropy wave generator of Bake *et al.* (2009a, b). Air of temperature T_o , density ρ_o and pressure $p_o = \rho_o RT_o$ flows at uniform speed U_o in a semi-infinite circular cylindrical duct of cross-sectional area A_1 into a converging-diverging nozzle that discharges smoothly into an infinite circular cylindrical duct of area A_2 . The flow is subsonic everywhere and is assumed to be isentropic.

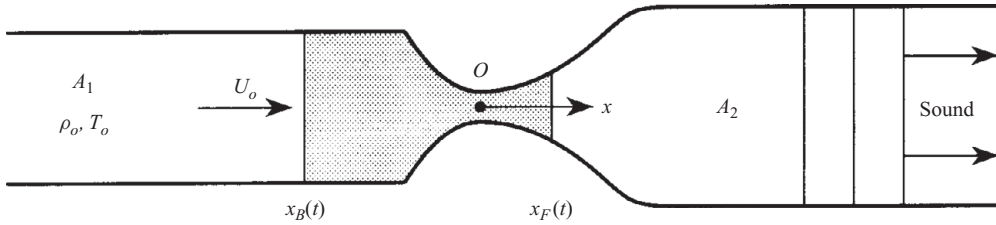


FIGURE 1. Schematic of the experiment performed by Bake *et al.* (2009a, b).

In this section attention is confined to the idealized case in which the inlet flow contains a uniform slug of heated air (shaded portion in figure 1) that is initially of uniform temperature $T_s > T_o$ and is at the local equilibrium pressure p_o and which convects steadily at the uniform flow velocity U_o . In the experiment $\Delta T = T_s - T_o$ is typically about 10°C and $\Delta T/T_o \ll 1$. Take the coordinate origin at O on the axis of symmetry at the nozzle throat, with the x axis in the direction of the mean flow. In a first approximation the mean flow is assumed to be quasi-one-dimensional, with the conditions uniform over each cross-section. The position of the heated slug at time t can then be specified by the x coordinates $x_F(t)$, $x_B(t)$, say, of the front and back faces of the slug, as indicated in figure 1.

Sound is generated because of the unsteadiness created when the slug is accelerated through the nozzle. Measurements reported by Bake *et al.* (2009a, b) indicate that the acoustic amplitude is proportional to $\Delta T/T_o$. This ratio determines the entropy excess of the hot slug relative to the ambient air. Because it is small it is sufficient to evaluate the entropy source on the right-hand side of (2.6) correct to $O(\Delta T/T_o)$. If the vortex source $\boldsymbol{\omega} \wedge \mathbf{v}$ in (2.6) is temporarily ignored, one can replace the variable coefficients involving ρ , c , T , \mathbf{v} in the equation by their local mean values, so that they may be regarded as functions of position alone within the nozzle.

Before the slug enters the nozzle the temperature distribution in the upstream duct is given by

$$T = T_o + \Delta T \{H(x_F(t) - x) - H(x_B(t) - x)\}, \tag{2.8}$$

where $H(\cdot)$ denotes the Heaviside step function, and the second term on the right-hand side is non-zero only within the interval $x_B < x < x_F$ occupied by the slug. Then the formula

$$s = c_p \ln T - R \ln p + \text{constant} \tag{2.9}$$

for the specific entropy of a perfect gas implies, to first order in $\Delta T/T_o$, that

$$\nabla s = \frac{c_p \Delta T}{T_o} \{\delta(x_B(t) - x) - \delta(x_F(t) - x)\} \mathbf{i}, \tag{2.10}$$

where \mathbf{i} is a unit vector in the x direction. This formula remains valid at all subsequent times as the slug convects through the nozzle, provided the motion is isentropic and the flow can be regarded as approximately one-dimensional.

Before the hot slug enters the nozzle, and before sound is produced, the entropy gradient (2.10) implies the existence of a corresponding gradient in the total enthalpy at the front and rear faces of the slug. According to definition (2.2) the initial distribution of $B \equiv B_o$, say, where $\nabla B_o = T_o \nabla s$. This gradient characterizes a non-acoustic variation of B that convects through the system at the variable mean flow velocity, and B_o represents an incoming solution of (2.6). Indeed, far upstream of the

nozzle (2.6) reduces to

$$-\nabla \cdot (\rho \nabla B_o) = -\nabla \cdot (\rho T_o \nabla s) \quad (2.11)$$

(because $DB_o/Dt=0$), and this relation is also satisfied during the passage of the slug through the contraction.

The acoustic component of B with outgoing wave behaviour is therefore isolated by putting

$$\hat{B} = B - B_o. \quad (2.12)$$

By recalling (refer to the end of §2.1) that the final monopole on the right-hand side of (2.6) can be neglected, we find that \hat{B} is determined by

$$\left(\rho \frac{D}{Dt} \left(\frac{1}{c^2} \frac{D}{Dt} \right) - \frac{\partial}{\partial x_j} \left(\rho \frac{\partial}{\partial x_j} \right) \right) \hat{B} = \text{div}(\rho \boldsymbol{\omega} \wedge \mathbf{v} - \rho(T - T_o) \nabla s), \quad (2.13)$$

which is to be solved subject to the condition that far from the contraction \hat{B} consists entirely of outgoing acoustic disturbances.

2.3. Solution using a Green's function

The nonlinear wave operator on the left-hand sides of (2.6) and (2.13) is self-adjoint (Möhring 1980; Howe 1998). The solution $\hat{B}(\mathbf{x}, t)$ of (2.13) can therefore be determined by using a Green's function that satisfies

$$\left(\rho \frac{D}{D\tau} \left(\frac{1}{c^2} \frac{D}{D\tau} \right) - \frac{\partial}{\partial y_j} \left(\rho \frac{\partial}{\partial y_j} \right) \right) G = \rho \delta(\mathbf{x} - \mathbf{y}) \delta(t - \tau), \quad G = 0 \text{ for } \tau > t, \quad (2.14)$$

where $\mathbf{y} = (x', y', z')$. Further, $G(\mathbf{x}, \mathbf{y}, t, \tau)$ is an 'advanced potential' that propagates as a function of (\mathbf{y}, τ) as an 'incoming' wave converging on the singularity at $\mathbf{y} = \mathbf{x}$ at time $\tau = t$ and vanishing thereafter. It is assumed that where ρ , c and \mathbf{v} occur explicitly and within the operator $D/D\tau$ in (2.14) they are to assume their steady values for undisturbed mean flow through the nozzle.

A formal representation of the solution of (2.13) can be obtained by the familiar procedure that leads to Kirchhoff's solution of the classical wave equation (Morse & Feshbach 1953; Baker & Copson 1969; Howe 1998). The variables (\mathbf{x}, t) in (2.13) are replaced by (\mathbf{y}, τ) , and the equation is multiplied by $G(\mathbf{x}, \mathbf{y}, t, \tau)$; this is subtracted from the product of $\hat{B}(\mathbf{y}, \tau)$ and (2.14), and the result is integrated over $-\infty < \tau < \infty$ and over the infinite fluid region V within the duct flow. By making use of the mean flow continuity equation $\text{div}(\rho \mathbf{v}) = 0$, it is found that

$$\begin{aligned} \rho \hat{B}(\mathbf{x}, t) &= \int_{-\infty}^{\infty} \frac{\partial}{\partial \tau} \int_V \frac{\rho}{c^2} \left(\hat{B} \frac{DG}{D\tau} - G \frac{D\hat{B}}{D\tau} \right) d^3 \mathbf{y} d\tau \\ &+ \int_{-\infty}^{\infty} \int_V \frac{\partial}{\partial y_j} \left(\rho G \frac{\partial \hat{B}}{\partial y_j} - \rho \hat{B} \frac{\partial G}{\partial y_j} \right) d^3 \mathbf{y} d\tau \\ &+ \int_{-\infty}^{\infty} \int_V \frac{\partial}{\partial y_j} \left(G \rho \left[(\boldsymbol{\omega} \wedge \mathbf{v})_j - (T - T_o) \frac{\partial s}{\partial y_j} \right] \right) d^3 \mathbf{y} d\tau \\ &- \int_{-\infty}^{\infty} \int_V \frac{\partial G}{\partial y_j} \rho \left[(\boldsymbol{\omega} \wedge \mathbf{v})_j - (T - T_o) \frac{\partial s}{\partial y_j} \right] d^3 \mathbf{y} d\tau. \end{aligned} \quad (2.15)$$

The first integral on the right-hand side vanishes identically because G and $DG/D\tau$ are both zero at $\tau = +\infty$, and causality implies that \hat{B} and $D\hat{B}/D\tau$ are null as $\tau \rightarrow -\infty$, at times τ prior to the passage of the entropy slug through the nozzle. The second

and third integrals are simplified by use of the divergence theorem, and the result is expressed in the form

$$\rho \hat{B}(\mathbf{x}, t) = \int_{-\infty}^{\infty} \oint_S \rho \left[\hat{B} \frac{\partial G}{\partial \mathbf{y}} - G \left(\frac{\partial \hat{B}}{\partial \mathbf{y}} + \boldsymbol{\omega} \wedge \mathbf{v} - (T - T_o) \frac{\partial s}{\partial \mathbf{y}} \right) \right] \cdot d\mathbf{S}(\mathbf{y}) d\tau \\ - \int_{-\infty}^{\infty} \int_V \rho \frac{\partial G}{\partial \mathbf{y}} \cdot \left(\boldsymbol{\omega} \wedge \mathbf{v} - (T - T_o) \frac{\partial s}{\partial \mathbf{y}} \right) d^3 \mathbf{y} d\tau, \quad (2.16)$$

where the surface integral is over the walls S of the upstream and downstream ducts and of the nozzle, with the surface element $d\mathbf{S}(\mathbf{y})$ directed into the fluid (causality and the definition of G rule out the possibility of any additional contributions from cross-sectional surface elements within the ducts at $x' = \pm\infty$).

By requiring Green's function to satisfy (2.14) subject to the condition that $\partial G / \partial y_n = 0$ on S , where y_n is a local normal coordinate on S , Crocco's equation (2.1) and the relation $\nabla B_o = T_o \nabla s$ permit the reduction of (2.16) to

$$\rho \hat{B}(\mathbf{x}, t) = \int_{-\infty}^{\infty} \oint_S \left[\rho G \frac{\partial \mathbf{v}}{\partial \tau} - \eta \frac{\partial G}{\partial \mathbf{y}} \wedge \boldsymbol{\omega} \right] \cdot d\mathbf{S}(\mathbf{y}) d\tau \\ - \int_{-\infty}^{\infty} \int_V \rho \frac{\partial G}{\partial \mathbf{y}} \cdot \left(\boldsymbol{\omega} \wedge \mathbf{v} - (T - T_o) \frac{\partial s}{\partial \mathbf{y}} \right) d^3 \mathbf{y} d\tau. \quad (2.17)$$

The surface integral can be discarded for isentropic flow in a rigid-walled duct. The remaining volume integral represents the leading approximation to the sound generated during the passage of the hot slug through the nozzle. The anomalous retention of the vortex source $\boldsymbol{\omega} \wedge \mathbf{v}$, when the frictional contribution from the surface integral in (2.17) has been discarded, is justified by the observation that although surface frictional forces over an extensive stretch of the wall S would normally produce a relatively low-frequency background contribution to the overall sound (as in Howe *et al.* 2006, for example), there exists the possibility of catastrophic and high-frequency production of vorticity by flow separation in the nozzle as a result of surface friction acting over a short section of the wall, and this could considerably influence the amplitude of the entropy noise.

The reduced form of (2.17) is used below to calculate the sound radiated within the duct at large distances from the nozzle. The mean flow Mach number far upstream and downstream of the nozzle satisfies $M^2 \ll 1$; this is the case in the experiments reported by Bake *et al.* (2009a, b), where the upstream Mach number $M_o = U_o / c_o \sim 0.03$. For subsonic nozzle flow the downstream Mach number is also negligible. In both cases the acoustic component of the pressure $p \simeq \rho \hat{B}$ and (2.17) can be applied in the form

$$p(\mathbf{x}, t) = - \int_{-\infty}^{\infty} \int_V \rho \frac{\partial G}{\partial \mathbf{y}} \cdot \left(\boldsymbol{\omega} \wedge \mathbf{v} - (T - T_o) \frac{\partial s}{\partial \mathbf{y}} \right) d^3 \mathbf{y} d\tau, \quad |\mathbf{x}| \rightarrow \infty. \quad (2.18)$$

3. Green's function

3.1. The compact approximation

An expression for the Green's function required to evaluate the solution (2.18) is derived in this section through the compact approximation, where the characteristic wavelength of the indirect combustion noise is much larger than the axial extent of the nozzle. This is appropriate for the subsonic experimental conditions of the experiments of Bake *et al.* (2007, 2009a, b), where the principal components of the indirect combustion noise produced in a nozzle of length ~ 0.3 m occurred

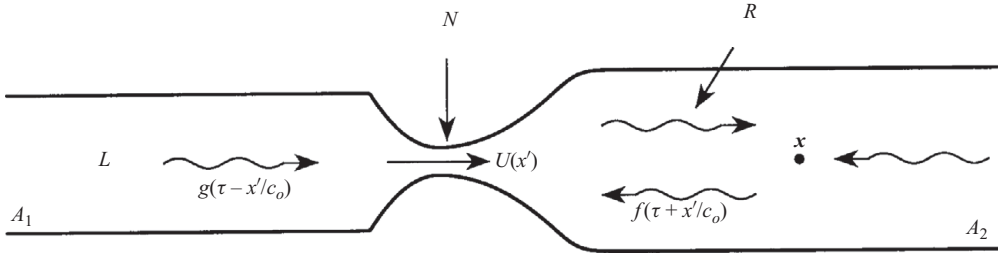


FIGURE 2. The regions L , N and R used in the definition of the compact Green's function.

at frequencies less than about 200 Hz. In these circumstances the unsteady motion determined by $G(\mathbf{x}, \mathbf{y}, t, \tau)$ (as a function of \mathbf{y} and τ) within the nozzle region N of figure 2 can be regarded as quasi-static, provided the field point \mathbf{x} on the right-hand side of (2.14) is several duct diameters from the nozzle. The details of the calculation of G are outlined in §§ 3.2 and 3.3; readers primarily concerned with applications to (2.18) may proceed directly to § 3.4 for a summary of the relevant formulae for G .

3.2. *Functional representations of $G(\mathbf{x}, \mathbf{y}, t, \tau)$ when x is large and positive*

Consider the determination of $G(\mathbf{x}, \mathbf{y}, t, \tau)$ governed by (2.14) when \mathbf{x} is downstream of the nozzle, as indicated schematically in figure 2. In the compact approximation the acoustic wavelengths are much larger than the duct diameter, and the flow duct is partitioned into the upstream and downstream regions respectively denoted by L and R in figure 2, where the mean flow Mach number $M = M_o$ is negligible, and the nozzle region N , where M will be permitted to assume high subsonic values.

The mean flow can be ignored in the downstream duct, where (2.14) becomes

$$\left(\frac{1}{c_o^2} \frac{\partial^2}{\partial \tau^2} - \frac{\partial^2}{\partial y_j^2} \right) G = \delta(\mathbf{x} - \mathbf{y})\delta(t - \tau), \quad G = 0 \quad \text{for } \tau > t, \quad (3.1)$$

where c_o is the locally uniform speed of sound in fluid of temperature T_o (taken to be the same as the undisturbed temperature in the upstream duct). Recalling the notation $\mathbf{y} = (x', y', z')$, with the x' axis in the mean flow direction along the axis of symmetry, it can be seen that in the long-wavelength approximation the solution in this region can be written as

$$G = \frac{c_o}{2A_2} H \left(t - \tau - \frac{|x - x'|}{c_o} \right) + f \left(\tau + \frac{x'}{c_o} \right), \quad (3.2)$$

provided $|x' - x|$ exceeds one or two duct diameters (Howe 1998). The first term on the right-hand side, involving the Heaviside step function, is just the corresponding compact Green's function in the absence of the nozzle, i.e. for an infinite duct of uniform cross-section A_2 . The plane wave $f(\tau + x'/c_o)$ arriving from $x' = +\infty$ takes account of the presence of the nozzle on the acoustic field 'imploding' into $\mathbf{y} = \mathbf{x}$ at time $\tau = t$.

We put $G = G_R$ in region R (where $x' < x$) between \mathbf{x} and the nozzle, where the approximation (3.2) is applicable, and write

$$G_R = \frac{c_o}{2A_2} H \left([t] - \tau + \frac{x'}{c_o} \right) + f \left(\tau + \frac{x'}{c_o} \right), \quad (3.3)$$

where $[t] = t - x/c_o$.

Similarly, in the upstream region L of uniform cross-section A_1 we can set $G = G_L$, where

$$G_L = g \left(\tau - \frac{x'}{c_o} \right) \quad (3.4)$$

is a plane wave arriving from $x' = -\infty$.

The quasi-static behaviour within the nozzle N is represented by $G = G_N$, where

$$G_N = \Phi(\tau) + \Psi(\tau)Y(\mathbf{y}). \quad (3.5)$$

The functions $\Phi(\tau)$, $\Psi(\tau)$ are to be determined, and $Y(\mathbf{y})$ must have vanishing normal derivative $\partial Y/\partial y_n$ on S and be a solution of the time-independent, homogeneous form of (2.14), i.e. of

$$\operatorname{div} \left(\frac{\mathbf{v}}{c^2} \operatorname{div}(\rho \mathbf{v} Y) - \rho \nabla Y \right) = 0, \quad (3.6)$$

where ρ , c , \mathbf{v} take their respective steady-state values $\rho(\mathbf{y})$, $c(\mathbf{y})$, $\mathbf{v}(\mathbf{y})$, with $\operatorname{div}(\rho \mathbf{v}) = 0$. This equation is simplified in the quasi-one-dimensional approximation by putting

$$\operatorname{div} \mathbf{Z} = \frac{1}{A(x')} \frac{\partial}{\partial x'} \int_{A(x')} Z_1 dy' dz' \simeq \frac{1}{A(x')} \frac{\partial}{\partial x'} (A(x') Z_1(x')) \quad (3.7)$$

for a vector field $\mathbf{Z} = (Z_1, Z_2, Z_3)$ that has vanishing normal component on the duct and nozzle wall, where the integration with respect to y' , z' is over the cross-section $A(x')$ of the duct, and variations of $Z_1(x')$ over this cross-section are assumed to be small.

Hence, (3.6) becomes

$$\frac{\partial}{\partial x'} \left(\rho A(x') (1 - M^2) \frac{\partial Y}{\partial x'} \right) = 0, \quad M = \frac{U(x')}{c(x')}, \quad (3.8)$$

where $U(x')$ is the cross-sectional mean of the axial velocity v_1 at x' . Therefore we can take

$$Y \equiv Y(x') = \int_0^{x'} \frac{\rho_o A_t d\xi}{\rho(\xi) A(\xi) [1 - M^2(\xi)]}, \quad (3.9)$$

where $\rho(\xi)$ and $M(\xi)$ are the mean density and Mach number at $x' = \xi$ in the duct and nozzle and A_t is the minimum cross-section at the nozzle throat. This normalization of Y implies that

$$Y(x') \sim \begin{cases} \frac{A_t}{A_2}(x' + \ell_2), & x' \rightarrow +\infty, \\ \frac{A_t}{A_1}(x' - \ell_1), & x' \rightarrow -\infty, \end{cases} \quad (3.10)$$

where the 'end corrections' ℓ_1 , ℓ_2 (Rayleigh 1945; Howe 1998) are given by

$$\ell_1 = \int_{-\infty}^0 \left(\frac{\rho_o A_1}{\rho A [1 - M^2]} - 1 \right) d\xi, \quad \ell_2 = \int_0^{\infty} \left(\frac{\rho_o A_2}{\rho A [1 - M^2]} - 1 \right) d\xi. \quad (3.11)$$

The order of magnitude of ℓ_1 , $\ell_2 \sim \wp A_{1,2}/A_t \gg \wp$, where \wp is similar to the maximum radius of curvature of the duct wall at the throat.

3.3. Equations for Φ , Ψ , f , g

The functional forms of Φ , Ψ , f , g are obtained in the compact approximation by equating the expansions of G_L , G_N , G_R to first order in x' in common

intervals of validity (Howe 1998, 2002; Howe & McGowan 2007). Thus in the region just downstream of the nozzle, at distances x' that are small compared with the characteristic acoustic wavelength in the entropy noise problem and where $M \ll 1$, we have $G_N \simeq G_R$, so that (3.3), (3.5) and (3.10) supply

$$\Phi + \frac{\Psi A_t}{A_2}(x' + \ell_2) = \frac{c_o}{2A_2}H([t] - \tau) + \frac{x'}{2A_2}\delta([t] - \tau) + f(\tau) + \frac{x'}{c_o}f'(\tau), \quad (3.12)$$

where $f' = df/d\tau$. Therefore,

$$\left. \begin{aligned} \Phi + \frac{\Psi A_t \ell_2}{A_2} &= f(\tau) + \frac{c_o}{2A_2}H([t] - \tau), \\ \frac{c_o \Psi A_t}{A_2} &= f'(\tau) + \frac{c_o}{2A_2}\delta([t] - \tau). \end{aligned} \right\} \quad (3.13)$$

Similarly, by matching the expansions of G_N and G_L upstream of the nozzle (where $M^2 \ll 1$), we find

$$\left. \begin{aligned} \Phi - \frac{\Psi A_t \ell_1}{A_1} &= g(\tau), \\ \frac{c_o \Psi A_t}{A_1} &= -g'(\tau). \end{aligned} \right\} \quad (3.14)$$

The system of equations (3.13) and (3.14) is readily solved, subject to the condition that the solution vanishes everywhere when $\tau > t$. In particular, we find

$$\left. \begin{aligned} \Phi &= \frac{c_o}{A_1 + A_2}H\left([t] - \tau - \frac{A_1(\ell_2 - \ell_1)}{c_o(A_1 + A_2)}\right), \\ \Psi &= \frac{A_1}{A_t(A_1 + A_2)}\delta\left([t] - \tau - \frac{(A_1\ell_2 + A_2\ell_1)}{c_o(A_1 + A_2)}\right). \end{aligned} \right\} \quad (3.15)$$

The substitution of these expressions into (3.5) determines the behaviour of $G \equiv G_N(\mathbf{x}, \mathbf{y}, t, \tau)$ when \mathbf{y} is in the vicinity of the nozzle for an observer at \mathbf{x} and at time t in the region far downstream of the nozzle. The representation (2.18) of the entropy noise indicates that only the space-dependent ('dipole') component $\Psi(\tau)Y(\mathbf{y})$ of (3.5) is required to evaluate the sound. On this understanding it is sufficient to adopt the following approximation for G for entropy sources in the nozzle region:

$$G(\mathbf{x}, \mathbf{y}, t, \tau) \simeq \frac{A_1 Y(x')}{A_t(A_1 + A_2)} \delta\left(t - \tau - \frac{x + \ell'}{c_o}\right), \quad x \rightarrow +\infty, \quad (3.16)$$

where $Y(x')$ is defined as in (3.9) and

$$\ell' = \frac{A_1\ell_2 + A_2\ell_1}{A_1 + A_2}. \quad (3.17)$$

3.4. Compact Green's function for the calculation of subsonic indirect combustion noise

A result similar to (3.16) is obtained for observer locations \mathbf{x} within the upstream duct. These various results for the effective compact Green's function for evaluation of the indirect combustion noise produced in the nozzle are summarized here for ease of reference:

$$G(\mathbf{x}, \mathbf{y}, t, \tau) \simeq \frac{\text{sgn}(x)A(-x)Y(x')}{A_t(A_1 + A_2)} \delta\left(t - \tau - \frac{|x| + \ell'}{c_o}\right), \quad |x| \rightarrow +\infty, \quad (3.18)$$

where $\mathbf{x} = (x, y, z)$; $\mathbf{y} = (x', y', z')$; ℓ' is defined as in (3.17) and (3.11); and

$$Y(x') = \int_0^{x'} \frac{\rho_o A_t d\xi}{\rho(\xi) A(\xi) [1 - M^2(\xi)]}. \quad (3.19)$$

4. Indirect combustion noise generated by an idealized hot slug

4.1. The entropy and vortex sound sources

The integral (2.18) for the acoustic pressure generated by the hot slug can now be evaluated. The passage of the temperature inhomogeneity through the nozzle must produce small-scale turbulence fluctuations in the diverging section. Proper design of the ‘diffuser’ section of the nozzle ensures that the Reynolds number is usually large enough and the angle of divergence of the diffuser small enough to prevent large-scale separation (Castillo, Wang & George 2004; Sparrow, Abraham & Minkowycz 2009), and it is only in exceptional cases that separation and ‘jetting’ occurs, but when it happens it can significantly modify the amplitude of the sound generated by the slug.

Both of these possible contributors to the indirect combustion noise are considered by writing the overall acoustic pressure in the form

$$p = p_s + p_\omega, \quad (4.1)$$

where the pressures on the right-hand side correspond respectively to the entropy gradient source $\partial s / \partial \mathbf{y}$ and the vortex sound source $\boldsymbol{\omega} \wedge \mathbf{v}$ in (2.18).

4.2. The entropy sound p_s

Consider the simple slug model of figure 1 and the sound radiated into the downstream duct. The entropy gradient $\partial s / \partial \mathbf{y}$ is given by (2.10), and $x > 0$ in formula (3.18) for the compact Green’s function. Then

$$\begin{aligned} p_s(x, t) &\simeq \int_{-\infty}^{\infty} \int_V \rho(T - T_o) \frac{\partial s}{\partial x'} \frac{\partial G}{\partial x'} d^3 \mathbf{y} d\tau \\ &= \rho_o \frac{A_1}{(A_1 + A_2)} \iint_{-\infty}^{\infty} \left(\frac{T - T_o}{1 - M^2(x')} \right) \frac{\partial s}{\partial x'}(x', \tau) \delta([t] - \tau) dx' d\tau \end{aligned} \quad (4.2a)$$

$$= \rho_o c_p \Delta T \frac{A_1}{(A_1 + A_2)} \int_{-\infty}^{\infty} \left(\frac{T(x')/T_o - 1}{1 - M^2(x')} \right) (\delta(x_B([t]) - x') - \delta(x_F([t]) - x')) dx', \quad (4.2b)$$

where $[t] = t - (x + \ell')/c_o$ is the effective retarded time.

This formula shows how the entropy sound received at time t is determined by the interaction of the entropy gradient at the retarded positions of the ends of the slug with the background mean flow variation of

$$\frac{T/T_o - 1}{1 - M^2} = \frac{-\frac{(\gamma - 1)}{2} M^2}{\left(1 + \frac{(\gamma - 1)}{2} M^2\right) (1 - M^2)}, \quad (4.3)$$

where the right-hand side is applicable for a perfect non-reacting gas for which γ is the ratio of the specific heats (Landau & Lifshitz 1987; Liepmann & Roshko 2002),

taken to be equal to 1.4 for air. Making this substitution in (4.2), and introducing the reference pressure $p_o = \rho_o RT_o$ of the flow far from the nozzle where the mean flow Mach number is negligible, we find

$$\frac{p_s}{p_o}(x, t) \simeq \frac{\Delta T}{T_o} \frac{A_1}{(A_1 + A_2)} \left(\left[\frac{\frac{\gamma}{2} M^2}{\left(1 + \frac{(\gamma-1)}{2} M^2\right) (1 - M^2)} \right]_F - \left[\frac{\frac{\gamma}{2} M^2}{\left(1 + \frac{(\gamma-1)}{2} M^2\right) (1 - M^2)} \right]_B \right), \quad x \rightarrow +\infty, \quad (4.4)$$

where the square brackets [] denote evaluation respectively at the retarded positions of the front and back faces of the entropy slug. These terms have very large peak values at the nozzle throat where $M \sim M_t$ is a maximum.

The downstream acoustic pressure profile accordingly consists of a positive pressure pulse generated as the front of the slug passes through the throat followed by a negative pulse of equal amplitude produced during the passage of the rear end of the slug. This is consistent with an increase in forward speed at the front of the slug, relative to its value for homogeneous flow at the higher ambient mean density, causing the nozzle throat to behave as an acoustic volume source of positive strength that radiates ahead of the slug. Similarly, relaxation of the increased forward speed during passage of the rear end of the slug causes the throat to behave as a negative acoustic source that radiates as an expansion wave. For subsonic flow each of the terms in square brackets in (4.4) attains its maximum value at the nozzle throat, where M is a maximum. The formula is valid only at subsonic Mach numbers in the approximation of (3.8).

An illustration of the waveform of the acoustic pressure predicted by (4.4) is shown in figure 3 for a maximum nozzle Mach number $M_t = 0.5$. The calculation has been performed for duct and nozzle-throat radii

$$R_1 = 15 \text{ mm}, \quad R_2 = 20 \text{ mm}, \quad R_t = 3.75 \text{ mm}. \quad (4.5)$$

These coincide with the corresponding values in the experiments of Bake *et al.* (2009*a, b*). The axial interval occupied by the nozzle is $-\ell_n < x < \ell_p$, and we take $\ell_n = 13 \text{ mm}$ ($= 0.867 R_1$) for the length of the convergent section, as in the experiment. However, for the discussion of this section the length ℓ_p of the diffuser has been set at $\ell_p = 4\ell_n = 52 \text{ mm}$, much shorter than the 253 mm diffuser used in the experiment. For these dimensions mean flow separation may occur in the nozzle, and the implications of this possibility are discussed in §4.3. The radius $r(x)$ of the nozzle cross-section is given by

$$r = \begin{cases} R_t + (R_1 - R_t)(x/\ell_n)^2, & -\ell_n < x \leq 0, \\ R_t + (R_2 - R_t)(x/\ell_p)^2, & 0 \leq x < \ell_p. \end{cases} \quad (4.6)$$

The front and back faces of the slug convect through the nozzle at approximately the speed $U(x)$ of the undisturbed mean flow, so that, for example, the position $x_F(t)$ of

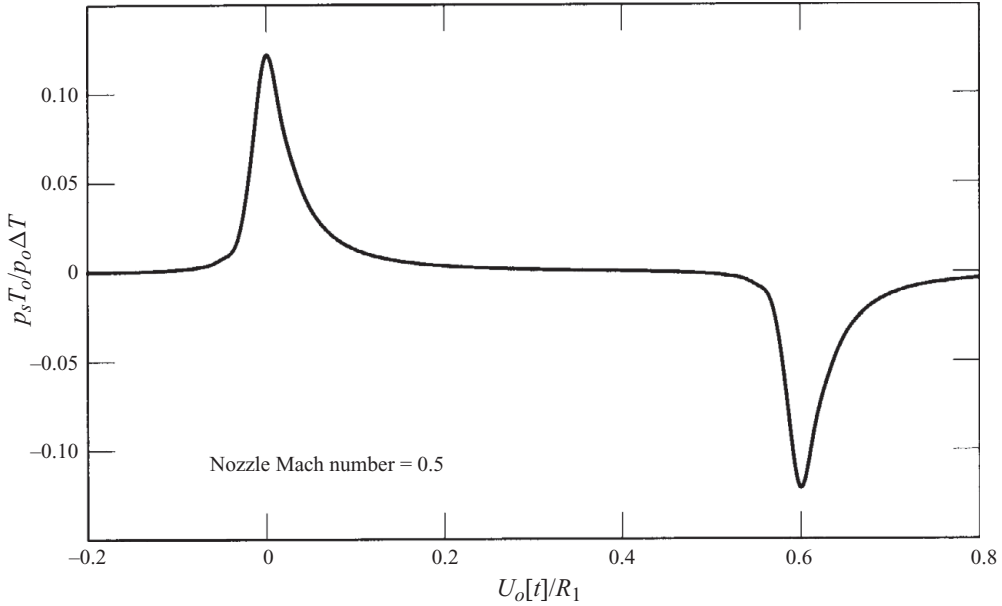


FIGURE 3. Typical downstream acoustic pressure profile (4.4) produced by the passage of an idealized entropy slug through the converging–diverging nozzle defined by (4.5) and (4.6) when $M_t = 0.5$.

the front at time t is determined by the equation

$$\frac{1}{U_o} \frac{dx_F}{dt} = \frac{U(x_F)}{U_o} = \frac{c}{c_o} \frac{M(x_F)}{M_o} = \frac{M(x_F)}{M_o \left(1 + \frac{\gamma - 1}{2} M^2(x_F)\right)^{1/2}}, \quad (4.7)$$

where (when $M_o^2 \ll 1$) the mean flow Mach number $M(x)$ is determined in terms of the cross-sectional area $A(x)$ by the quasi-one-dimensional formula for steady isentropic flow (Landau & Lifshitz 1987; Liepmann & Roshko 2002),

$$\frac{M(x)}{\left(1 + \frac{\gamma - 1}{2} M^2(x)\right)^{(\gamma+1)/2(\gamma-1)}} = \frac{M_o A_1}{A(x)}. \quad (4.8)$$

Equation (4.7) is readily solved numerically by Runge–Kutta integration.

In figure 3 the normalized acoustic pressure $p_s T_o / p_o \Delta T$ radiated into the downstream duct is plotted against the non-dimensional retarded time $U_o [t] / R_1$, where time is measured from the instant at which the front of the slug passes through the throat. In the present case the nozzle-throat Mach number $M_t = 0.5$ corresponds to a uniform flow in the upstream duct at speed $U_o \simeq 9.2 \text{ m s}^{-1}$. The slug length has been set arbitrarily to equal $0.6R_1 = 9 \text{ mm}$, so that the positive and negative peaks of the pressure wave are separated by a retarded time difference $U_o [\delta t] / R_1 \simeq 0.6$, corresponding to the difference in the arrival times at the throat of the front and back faces of the slug.

Figure 4 illustrates the predicted variation of the peak acoustic pressure of the first pulse (at $U_o [t] / R_1 \sim 0$) with the nozzle-throat Mach number M_t (calculated by

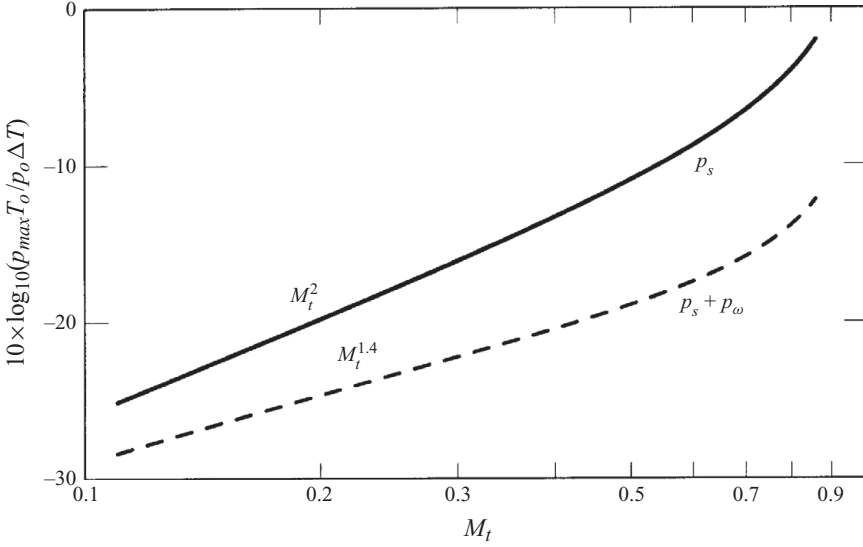


FIGURE 4. Dependence on throat Mach number M_t of the indirect entropy-generated sound in the converging–diverging nozzle defined by (4.5) and (4.6): continuous line, peak downstream pressure p_s for an idealized entropy slug (see (4.4)); dashed line, peak downstream pressure $p_s + p_\omega$ for the slug accompanied by vortex shedding in the nozzle (see (4.18)).

putting $M = M_t$ in the first bracketed term $[\cdot]_F$ of (4.4). Evidently the peak pressure increases like M_t^2 until about $M_t \sim 0.5$, after which nonlinearity becomes important.

4.3. Contribution from separated flow in the diffuser

Isentropic theory ignores the production of vorticity within the flow and small-scale turbulence generated in the boundary layers. However, it would not be permissible to neglect the shedding of large-scale coherent distributions of vorticity from the walls, i.e. separation. This should not occur in a properly designed converging–diverging nozzle, except possibly at lower Reynolds numbers outside the design envelope. For the short, wide-angle diffuser of § 4.2 (of divergence angle $\sim 35^\circ$) separation might be expected to occur in the diffuser over a wide range of large Reynolds numbers (Castillo *et al.* 2004; Sparrow *et al.* 2009), leading to jet formation in which vorticity in the jet shear layer is modulated in strength by the passage of the hot slug. It is difficult to give a fully satisfactory theory of sound production by this vorticity, but a very approximate prediction can be made by consideration of the simplified model illustrated in figure 5(a), where separation is assumed to occur at the throat, producing a uniform jet of circular cross-section and area $\simeq A_t$.

The vortex source term $\boldsymbol{\omega} \wedge \mathbf{v}$ in (2.18) can be estimated by the method of Howe (1998, § 3.2.3) and Howe & McGowan (2007), who assumed that the large-scale coherent jet vorticity is confined to a free shear layer of infinitesimal thickness – a cylindrical vortex sheet. The vortex sheet has circulation U_j per unit length of the jet, where $U_j(x, t)$ is the jet speed, which is uniform over the jet cross-section, and the shear layer vorticity is convected by the flow at speed $U_j/2$. Then $\boldsymbol{\omega} \wedge \mathbf{v} = (1/2)U_j^2 \delta(s_\perp) \mathbf{n}$, where s_\perp is measured from the vortex sheet in the direction of its outward unit normal \mathbf{n} (figure 5a), so that the vortex sound pressure p_ω is given by

$$p_\omega \simeq -\frac{1}{2} \int_{-\infty}^{\infty} \int_{S_j} \rho U_j^2 \frac{\partial G}{\partial y_n} dS(\mathbf{y}) d\tau, \quad (4.9)$$

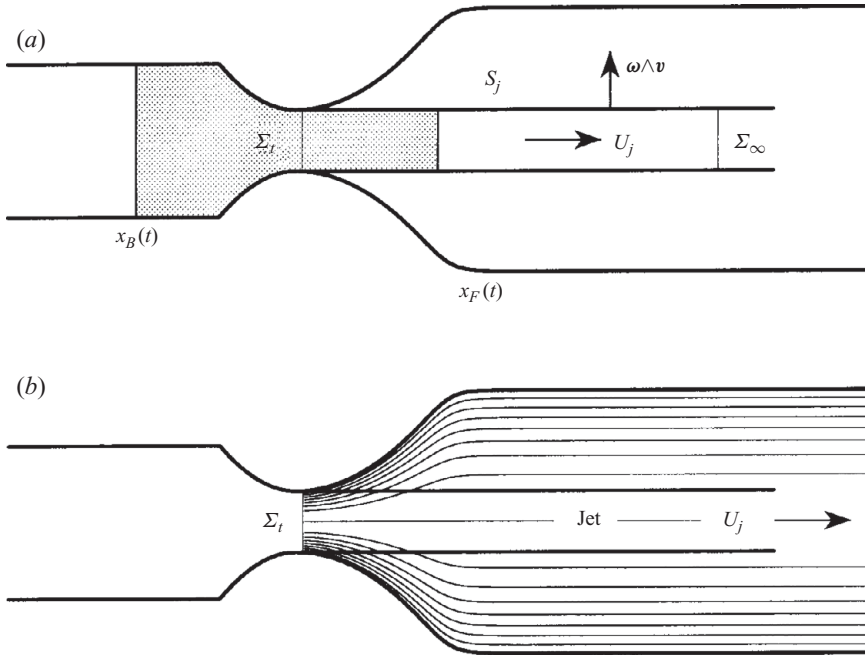


FIGURE 5. (a) Simplified model for estimating the vortex sound produced when separation and jet formation occur at the nozzle. (b) Illustration of the streamline pattern defined by the vector field ∇Y .

where the surface integral is over the cylindrical vortex sheet S_j . It may be verified from (3.3) and (3.18) that only that part of the jet that is within about one duct diameter from the nozzle can contribute to the integral, where G can be taken in the form given in (3.18), so that

$$p_\omega(x, t) \simeq - \frac{A_1}{2A_t(A_1 + A_2)} \int_{S_j} U_j^2(x', [t]) \rho \frac{\partial Y}{\partial y_n} dS(\mathbf{y}), \quad x \rightarrow +\infty. \quad (4.10)$$

Indeed, the main contribution to the integral is from those regions of S_j where $\nabla Y(\mathbf{y})$ has a significant component normal to the cylindrical jet shear layer (see figure 5b). Because $\partial Y / \partial y_n = 0$ on the nozzle wall, $\partial Y / \partial y_n \neq 0$ on S_j only within a short interval just downstream of the throat. A qualitative picture of this is obtained by considering the family of ‘streamlines’ of the ‘flow’ whose velocity is ∇Y when $M=0$ (or $M^2 \ll 1$) in the definition (3.9), when Y satisfies $\nabla^2 Y = 0$, the limiting form of (3.6) at $M=0$. The corresponding Stokes stream function for this flow is $\psi(x, \varpi) \simeq (1/2)A_t \varpi^2 / A(x)$ (where ϖ is the radial distance from the x axis of symmetry; see Batchelor 1967; Landau & Lifshitz 1987). The pattern of the family of streamlines, $\psi(x, \varpi) = \text{constant}$, is depicted in figure 5(b); they diverge rapidly downstream of the throat and are essentially parallel to the jet within a distance of about one duct diameter.

At the lower frequencies that are known to dominate indirect combustion noise it is permissible to neglect the variation with x' of $U_j(x', [t])$ over the region of integration in (4.10), which becomes

$$p_\omega(x, t) \simeq - \frac{A_1 U_j^2(0, [t])}{2A_t(A_1 + A_2)} \int_{S_j} \rho \frac{\partial Y}{\partial y_n} dS(\mathbf{y}), \quad x \rightarrow +\infty. \quad (4.11)$$

The remaining integral is evaluated by integrating (3.6) over the volume of the jet between the cross-sections Σ_t and Σ_∞ indicated in figure 5(a) and applying the divergence theorem. This yields (using the approximation (3.9))

$$\int_{S_j} \rho \frac{\partial Y}{\partial y_n} dS(\mathbf{y}) = \int_{\Sigma_t + \Sigma_\infty} (M^2 - 1) \rho \frac{\partial Y}{\partial y_n} dS \simeq \rho_o A_t, \quad (4.12)$$

so that the vortex sound contribution becomes

$$p_\omega(x, t) \simeq - \frac{A_1 \rho_o U_j^2(0, [t])}{2(A_1 + A_2)}, \quad x \rightarrow +\infty. \quad (4.13)$$

To make explicit numerical estimates it remains to evaluate the time-dependent component of the jet speed $U_j(0, [t])$ at the throat.

4.4. The overall indirect combustion noise

The sound pressure radiated downstream of the nozzle now becomes

$$p(x, t) = p_s(x, t) + p_\omega(x, t) \quad (4.14)$$

in which the terms on the right-hand side are given respectively by (4.4) and (4.13), which define plane acoustic waves having wavelengths much larger than the diameter of the downstream duct, where the density and sound speed are respectively equal to ρ_o and c_o .

Now

$$U_j(0, [t]) = U_t + U_s, \quad (4.15)$$

where U_t is the mean flow velocity at the throat and $U_s \equiv U_s([t])$ is the perturbation produced by the production of sound. When the acoustic wavelength is large compared with all other dimensions of the problem the velocity U_s can be estimated in terms of the limiting value of the

$$\text{acoustic particle velocity} \equiv V(t) = \lim_{x \rightarrow +\infty} \frac{p(x, t)}{\rho_o c_o} \quad (4.16)$$

by equating the unsteady volume flux $V A_2$ in the acoustically compact region just downstream of the nozzle to the jet volume flux $U_s A_t$ (Lighthill 1978). Then, the linearized, unsteady component of (4.13) (obtained by replacing U_j^2 by $2U_s U_t$) and the near-field form of (4.14) supply

$$V(t) \simeq \frac{p_s(0, t)}{\rho_o c_o \left[1 + \frac{A_1}{(A_1 + A_2)} \frac{A_2}{A_t} M_t \left(1 + \frac{(\gamma - 1)}{2} M_t^2 \right)^{1/2} \right]}. \quad (4.17)$$

But the acoustic pressure in the downstream region $p(x, t) = \rho_o c_o V([t])$. Hence the indirect combustion noise (4.14) with inclusion of the effects of separation at the nozzle is given by

$$p(x, t) \simeq \frac{p_s(x, t)}{\left[1 + \frac{A_1}{(A_1 + A_2)} \frac{A_2}{A_t} M_t \left(1 + \frac{(\gamma - 1)}{2} M_t^2 \right)^{1/2} \right]}, \quad x \rightarrow +\infty. \quad (4.18)$$

The effect of vortex shedding is therefore to produce a uniform decrease in the overall sound pressure relative to $p_s(x, t)$, generated when separation is absent or ignored, by a factor determined by the denominator in this formula. In particular

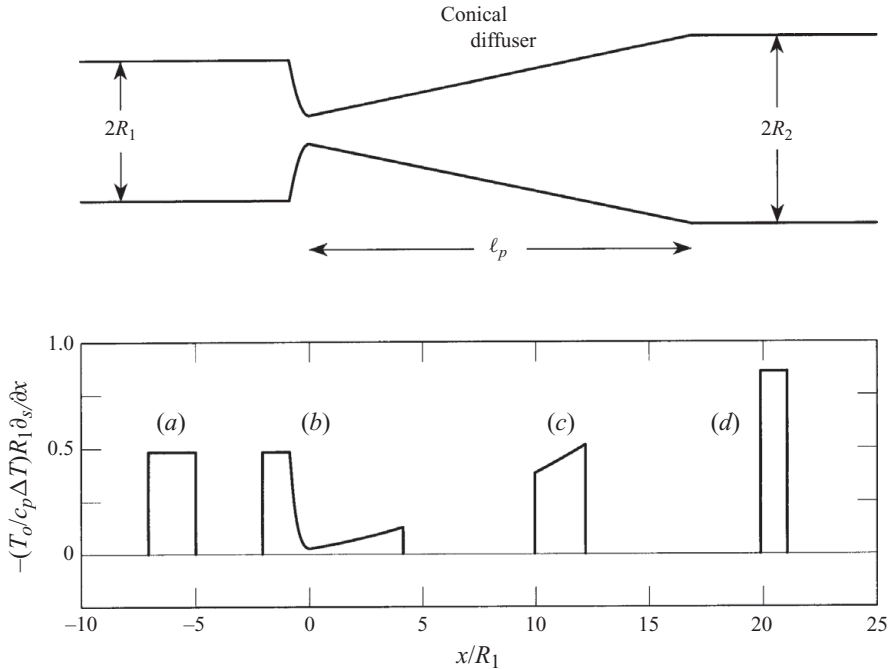


FIGURE 6. The converging–diverging nozzle used in the experiments of Bake *et al.* (2009*b*). The lower part of the figure depicts changes in the entropy gradient in the front transition region at $x \sim x_F(t)$ as it convects through the nozzle, for a case in which the initial gradient (a) is constant. The minimum in case (b) occurs at the throat at $x/R_1=0$. Cases (c) and (d) illustrate the progressive contraction of the transition region within the diffuser, the entropy gradient at (d) in the uniform downstream duct relaxing to a new constant value. For $M_t=0.6$ and an initial wave front rise time, $l_F/U_o = 3$ ms.

there is a systematic reduction in the maximum acoustic pressure p_{max} produced as the front face of the entropy slug passes through the throat, as indicated by the dashed line in figure 4. At lower Mach numbers the maximum pressure is now seen to vary approximately as $M_t^{1.4}$.

This conclusion is of interest because (as discussed in more detail in §5) the experiments of Bake *et al.* (2009*a, b*) revealed that the maximum entropy noise sound pressure peaks at a nozzle Mach number $M_t \sim 0.6$, beyond which it has a tendency to decrease. The results of figure 4 imply that although vorticity production reduces the acoustic amplitudes, it cannot apparently account for the observed progressive decline at high Mach numbers.

5. Indirect combustion noise measured by Bake *et al.* (2009*b*)

The experiments of Bake *et al.* (2009*b*) were performed using a nozzle similar to that described in §4 (with dimensions (4.5)), but with the short downstream section replaced by a long conical diffuser of length $\ell_p = 253$ mm, as illustrated in the upper part of figure 6. A succession of entropy slugs was produced by passing the air through a bank of pulsed electrical elements in the upstream duct, which heated the flow periodically every second for 100 ms. Through this the axial temperature distribution within the slug could be ‘shaped’ by imposing suitable time delays between different heating elements. However, in their comprehensive discussion of the

experiments, Bake *et al.* (2009b) supplied details for only two slugs having a nominally uniform entropy excess $\sim c_p \Delta T / T_o$, corresponding to the ideal model defined by (2.8), except that the step-like discontinuities in specific entropy at the front and back faces of the slug now occur smoothly over transition regions of finite widths. It will be seen below that acoustic predictions based on the idealized model (2.8) agree with experiment only at very low Mach numbers; at higher Mach numbers it is necessary to take account of the finite ‘rise time’ of the entropy wave profile at its ends.

It will be assumed for simplicity that the temperature varies linearly across these transition zones. The initial variation of the perturbation entropy across, for example, the front of the slug can then be represented approximately by the formula

$$s \simeq \frac{c_p \Delta T}{T_o} \frac{(x_F(0) - x)}{l_F(0)}, \quad x_F(0) - l_F(0) < x < x_F(0), \quad (5.1)$$

where $l_F(0)$ is the width of the transition region when the slug is upstream of the nozzle at some initial instant that we take to correspond to $t = 0$. This length will change during passage through the nozzle because the mean flow convection velocities are different at the front $x = x_F(t)$ and the back $x = x_F(t) - l_F(t)$ of the transition region. The positions of these points at time $t > 0$ are easily found by integration of an equation of the form (4.7).

The sound produced in the downstream duct during the passage of the entropy wavefront through the nozzle is calculated using (4.2a) in terms of the entropy gradient at the retarded position of the front transition region. The gradient is determined by appeal to the mean flow Jacobian formula $\rho(x')A(x')dx' = \rho_o A_1 dx$ relating the length differential dx' of a fluid element at x' in the nozzle at time τ to its length dx at the initial position of the transition zone at time $\tau = 0$, so that

$$\frac{\partial s}{\partial x'}(x', \tau) = \frac{\partial s}{\partial x}(x, 0) \frac{\rho(x')A(x')}{\rho_o A_1} \equiv -\frac{c_p \Delta T}{l_F(0)T_o} \frac{\rho(x')A(x')}{\rho_o A_1}, \quad x_F(\tau) - l_F(\tau) < x' < x_F(\tau). \quad (5.2)$$

Hence, using (4.3) and the isentropic mean flow relation (Liepmann & Roshko 2002)

$$\frac{\rho(x')A(x')}{\rho_o A_1} \simeq \frac{M_o}{M} \left(1 + \frac{(\gamma - 1)}{2} M^2 \right)^{1/2}, \quad \text{where } M = M(x') \text{ and } M_o^2 \ll 1, \quad (5.3)$$

we find

$$\frac{p_s}{p_o}(x, t) \simeq \frac{\Delta T}{T_o} \frac{A_1}{(A_1 + A_2)} \frac{\gamma M_o}{2l_F(0)} \int_{x_F(t) - l_F(t)}^{x_F(t)} \frac{M dx'}{\left(1 + \frac{(\gamma - 1)}{2} M^2 \right)^{1/2} (1 - M^2)}, \quad x \rightarrow +\infty. \quad (5.4)$$

This formula determines the positive acoustic pressure pulse generated as the slug passes through the nozzle, which exhibits a wave profile that resembles, but is generally much broader than, the positive pressure pulse of figure 3 for the idealized slug. A similar expression can be written for the expansion wave generated by the rear transition region at $x \sim x_B(t)$.

When $l_F(0) \rightarrow 0$, (5.4) yields predictions for the peak acoustic pressure that coincide with the curve labelled p_s in figure 4, for the idealized entropy slug with the gradient given by (2.10). When $l_F \neq 0$, however, there are significant changes in both the amplitude and the detailed wave profile of the sound, particularly at higher Mach numbers. This is because the transition regions at the front and back faces of the

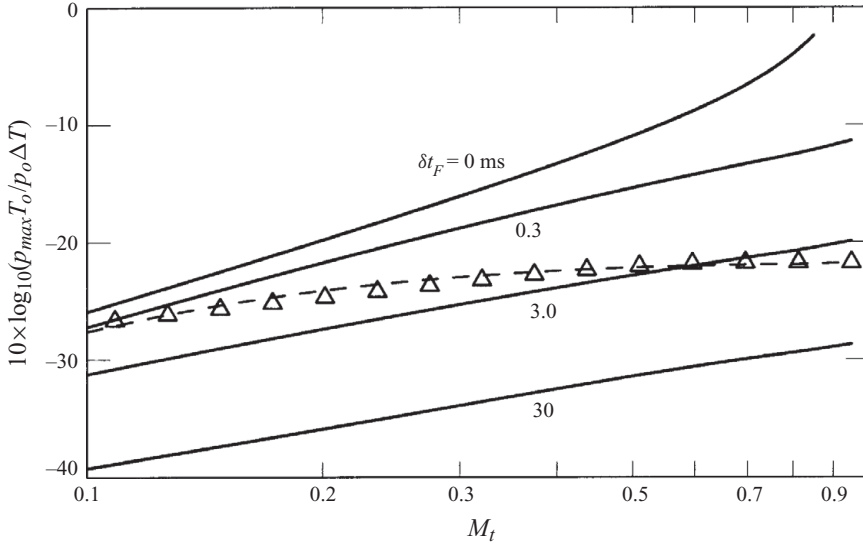


FIGURE 7. The predicted peak acoustic pressure (continuous line) of the indirect entropy sound generated by slug flow through a converging–diverging nozzle of the type used in the experiments of Bake *et al.* (2009*b*) for different initial entropy wavefront rise times δt_F ; triangles, the peak pressure measured by Bake *et al.* (2009*b*); dashed line, the predicted peak pressure when the initial rise time $\delta t_F = 3(M_t/0.6)$ ms.

slug are stretched out along the nozzle because of the rapid spatial variations of the mean flow speed in the neighbourhood of the throat. The stretching of the front transition region and the corresponding changes in the entropy gradient $\partial s/\partial x$ within the transition zone are illustrated in figure 6 when the throat Mach number $M_t = 0.6$ (so that $U_o \simeq 10.35 \text{ m s}^{-1}$) and when the initial width $l_F(0) \simeq 30 \text{ mm}$ ($\equiv 2R_1$) in the upstream duct, where the initial non-dimensional entropy gradient $-(T_o/c_p \Delta T)R_1 \partial s/\partial x \equiv R_1/l_F(0) \simeq 0.49$. In case (a) of figure 6 the front and the back of the transition region are respectively at $x/R_1 = -5$ and $x/R_1 = -7$.

In case (b) of figure 6 the front transition region is stretched over more than three duct diameters between $x/R_1 \simeq -2.06$ and $x/R_1 \simeq +4.13$, causing the entropy gradient to have a sharp and small minimum at the throat, i.e. at the precise location at which the peak sound pressure is generated by an idealized, sharp-fronted entropy slug. The behaviour of the transition region at later times is not acoustically significant, but cases (c) and (d) of figure 6 show how the transition zone gradually contracts as the mean flow velocity decreases at the front $x = x_F$, and the entropy gradient across the front progressively increases as it traverses the diffuser, finally attaining a uniform non-dimensional value $\sim 0.86 = (R_1/l_F(0))(A_2/A_1)$.

This stretching of the transition regions is increased further at higher Mach numbers (so that gradient amplitudes are reduced relative to those shown in figure 6), and this tends to counteract the growth in the maximum acoustic wave amplitude associated with the factor $1/(1 - M^2)$ in the integral of (5.4). This is illustrated in figure 7, where the variation of the maximum acoustic pressure radiated downstream is plotted (continuous line) as a function of the throat Mach number for different initial values of the entropy wavefront rise time $\delta t_F = l_F(0)/U_o$, namely for $\delta t_F = 0, 0.3, 3.0, 30.0$ ms. The case $\delta t_F = 0$ corresponds to the idealized hot slug of §4. The results confirm the dramatic reduction in wave amplitude produced by an elongated transition region,

exacerbated by stretching of the front in the nozzle. Note that although the present theory is formally inapplicable when $M_t \rightarrow 1$, the plots for $\delta t_F > 0$ do not exhibit singular behaviour associated with the singularity of (5.4) at $M(x') = 1$ at the throat. This is because the growth of the singularity is countered by stretching, which causes the entropy gradient to be very small at the throat, and it is not until M_t is very close to unity that the singularity becomes apparent.

Bake *et al.* (2009*b*) presented results for $M_t = 0.7, 1$ for which the initial rise times δt_F appear to be respectively of orders 10 and 30 ms. They also presented experimental data for the variation of the peak pressure with throat Mach number, which is reproduced in figure 7 (triangles). Actually the data points do not fall on a single curve, and our plot is a 'best fit', corresponding the curve labelled (in our notation) $M_t^{0.74}$ in figure 8 of Bake *et al.* (2009*b*) and its extrapolation to $M_t \sim 1$.

The experimental data exhibit a weak maximum near $M_t \sim 0.6$, and the subsequent decrease in peak pressure at higher Mach numbers appears anomalous and has not hitherto been explained by the numerical simulations reported in Bake *et al.* (2009*b*). They have given no detailed information about the geometrical properties of the entropy slugs. In particular, no data are available for the rise time δt_F of the entropy wavefront. However, the very limited discussion of this in Bake *et al.* (2009*b*) suggests that in the experiments δt_F increases with the throat Mach number M_t . According to figure 7 the measured peak pressure at low Mach numbers is close to those predicted by ideal slug theory and by (5.4) for $\delta t_F = 0.3$ ms. The measurements evidently imply that δt_F increases with M_t , and the simple empirical model

$$\delta t_F \simeq 0.003 \times \frac{M_t}{0.6} \quad (\text{in seconds}) \quad (5.5)$$

appears to represent well what might be deduced from the intersection of the measurement curve in figure 7 with the prediction curves for $\delta t_F = 0.3$ and 3.0 ms. The formula supplies $\delta t_F = 3$ ms at $M_t = 0.6$; at $M_t = 0.1$ it yields $\delta t_F = 0.5$ ms.

The dashed line curve in figure 7 is the prediction of (5.4) when the initial rise time is given by (5.5). The agreement up to $M_t = 0.6$ is to be expected. More surprisingly, perhaps, is the flattening off of the predictions above $M_t = 0.6$, which is also in accord with experiment.

6. Conclusion

Indirect combustion noise is associated with the passage of nominally quiescent temperature/entropy inhomogeneities or 'hot spots' through regions of rapidly accelerated mean flow. The subject has been studied for many years and is known to be important for a proper understanding of jet engine noise. The recent canonical experiments performed by Bake *et al.* (2009*b*) using an entropy wave generator coupled with a converging-diverging nozzle have aroused renewed interest in the theory, in particular because of the apparent anomalous measured behaviour, according to which the sound level produced by a slug of hot gas is found to peak at a relatively low nozzle Mach number of about 0.6. Our application of the acoustic analogy theory to a simplified version of this problem indicates that two important mechanisms control the amplitude of the sound produced by a nominally uniform slug of hot gas. First, in cases in which flow separation occurs in the diffuser section of the nozzle, manifested by the formation of a jet whose large-scale shear layer vorticity is modulated by the hot slug, the vortex sound produced is strongly correlated with the entropy noise and can dramatically reduce the overall sound level,

especially at higher subsonic Mach numbers, where the peak acoustic power can be decreased by 10–20 dB. Second, streamwise deformation of the hot slug during rapidly varying acceleration in the mean nozzle flow significantly reduces the entropy gradients within the front and rear interfaces, especially in the vicinity of the throat, which is the principal source of the entropy noise. It appears that this rapid distortion of the flow is responsible for the decrease in acoustic pressure observed by Bake *et al.* (2009*b*) at high subsonic Mach numbers. However, confirmation of this conjecture will probably require many of their tests to be repeated to permit data concerning slug distortion to be properly quantified.

The author expresses his gratitude to Dr Friedrich Bake for supplying details of the entropy wave generator used in the experiments of Bake *et al.* (2009*b*).

REFERENCES

- BAKE, F., KINGS, N., FISCHER, A. & ROHLE, I. 2009*a* Experimental investigation of the entropy noise mechanism in aero-engines. *Intl J. Aeroacoust.* **8**, 125–141.
- BAKE, F., MICHEL, U. & ROHLE, I. 2007 Investigation of entropy noise in aeroengine combustors. *J. Engng Gas Turbines Power* **129**, 370–376.
- BAKE, F., RICHTER, C. MUHLBAUER, B., KINGS, N., ROHLE, I., THIELE, F. & NOLL, B. 2009*b* The entropy wave generator (EWG): a reference case on entropy noise. *J. Sound Vib.* **326**, 574–598.
- BAKER, B. B. & COPSON, E. T. 1969 *The Mathematical Theory of Huygens' Principle*, 2nd edn. Oxford University Press.
- BATCHELOR, G. K. 1967 *An Introduction to Fluid Dynamics*. Cambridge University Press.
- BLOY, A. W. 1979 The pressure waves produced by the convection of temperature disturbances in high subsonic nozzle flows. *J. Fluid Mech.* **94**, 465–475.
- BOHN, M. S. 1977 Response of a subsonic nozzle to acoustic and entropy disturbances. *J. Sound Vib.* **52**, 283–297.
- CANDEL, S. M. 1972 Analytical studies of some acoustic problems of jet engines. PhD thesis, California Institute of Technology, Pasadena, CA.
- CASTILLO, L., WANG, X. & GEORGE, W. K. 2004 Separation criterion for turbulent boundary layers via similarity analysis. *Trans. ASME J. Fluids Engng* **126**, 297–304.
- CRIGHTON, D. G., DOWLING, A. P., FLOWCS WILLIAMS, J. E., HECKL, M. & LEPPINGTON, F. G. 1992 *Modern Methods in Analytical Acoustics (Lecture Notes)*. Springer.
- CUMPSTY, N. A. 1979 Jet engine combustion noise: pressure, entropy and vorticity perturbations produced by unsteady combustion or heat addition. *J. Sound Vib.* **66**, 527–544.
- CUMPSTY, N. A. & MARBLE, F. E. 1977*a* Core noise from gas turbine exhausts. *J. Sound Vib.* **54**, 297–309.
- CUMPSTY, N. A. & MARBLE, F. E. 1977*b* The interaction of entropy fluctuations with turbine blade rows; a mechanism of turbojet engine noise. *Proc. R. Soc. Lond. A* **357**, 323–344.
- FLOWCS WILLIAMS, J. E. & HOWE, M. S. 1975 The generation of sound by density inhomogeneities in low Mach number nozzle flows. *J. Fluid Mech.* **70**, 605–622.
- HOWE, M. S. 1975 Contributions to the theory of aerodynamic sound, with application to excess jet noise and the theory of the flute. *J. Fluid Mech.* **71**, 625–673.
- HOWE, M. S. 1998 *Acoustics of Fluid–Structure Interactions*. Cambridge University Press.
- HOWE, M. S. 2002 *Theory of Vortex Sound*. Cambridge University Press.
- HOWE, M. S., IIDA, M., MAEDA, T. & SAKUMA, Y. 2006 Rapid calculation of the compression wave generated by a train entering a tunnel with a vented hood. *J. Sound Vib.* **297**, 267–292.
- HOWE, M. S. & MCGOWAN, R. S. 2007 Sound generated by aerodynamic sources near a deformable body, with application to voiced speech. *J. Fluid Mech.* **592**, 367–392.
- LANDAU, L. D. & LIFSHITZ, E. M. 1987 *Fluid Mechanics*, 2nd edn. Oxford University Press.
- LEYKO, M., NICOU, F., MOREAU, S. & POINSOT, T. 2009 Numerical and analytical investigation of the indirect combustion noise in a nozzle. *C. R. Mec.* **337**, 415–425.
- LEYKO, M., NICOU, F. & POINSOT, T. 2009 Comparison of direct and indirect combustion noise mechanisms in a model combustor. *AIAA J.* **47**, 2709–2716.

- LIEPMANN, H. W. & ROSHKO, A. 2002 *Elements of Gas Dynamics*. Dover.
- LIGHTHILL, J. 1978 *Waves in Fluids*. Cambridge University Press.
- LIGHTHILL, M. J. 1952 On sound generated aerodynamically. Part I: general theory. *Proc. R. Soc. Lond. A* **211**, 564–587.
- LU, H. Y. 1977 An analytical model for entropy noise of subsonic nozzle flow. *AIAA Paper* 77-1366.
- MARBLE, F. E. 1973 Acoustic disturbances from gas nonuniformities convected through a nozzle. In *Interagency Symposium on University Research in Transportation Noise*, Stanford University, Stanford, CA.
- MARBLE, F. E. & CANDEL, S. M. 1977 Acoustic disturbance from gas non-uniformities convected through a nozzle. *J. Sound Vib.* **55**, 225–243.
- MÖHRING, W. 1980 Modelling low Mach number noise. In *Mechanics of Sound Generation in Flows* (ed. E.-A. Muller), pp. 85–96. Springer.
- MORFEY, C. L. 1973 Amplification of aerodynamic noise by convected flow inhomogeneities. *J. Sound Vib.* **31**, 391–397.
- MORSE, P. M. & FESHBACH, H. 1953 *Methods of Theoretical Physics*. McGraw-Hill.
- MUHLBAUER, B., NOLL, B. & AIGNER, M. 2009 Numerical investigation of the fundamental mechanism for entropy noise generation in aero-engines. *Acta Acust. United Acust.* **95**, 470–478.
- MUTHUKRISHNAN, M., STRAHLE, W. & NEALE, D. 1978 Separation of hydrodynamic, entropy, and combustion noise in a gas turbine combustor. *AIAA J.* **16**, 320–327.
- POINSOT, T. & VEYNANTE, D. 2005 *Theoretical and Numerical Combustion*, 2nd edn. R. T. Edwards.
- RAYLEIGH, L. 1945 *Theory of Sound*, vol. 2. Dover.
- SPARROW, E. M., ABRAHAM, J. P. & MINKOWYCZ, W. J. 2009 Flow separation in a diverging conical duct: Effect of Reynolds number and divergence angle. *Intl J. Heat Transfer* **52**, 3079–3083.
- STRAHLE, W. C. 1971 On combustion generated noise. *J. Fluid Mech.* **49**, 399–414.
- STRAHLE, W. C. 1978 Combustion noise. *Prog. Energy Combust. Sci.* **4**, 157–176.
- ZUKOSKI, E. E. & AUERBACH, J. M. 1976 Experiments concerning the response of supersonic nozzles to fluctuating inlet conditions. *ASME J. Engng Power*, **98**, 60–63.